Nanoconfinement Facilitates Reactions of Carbon Dioxide in Supercritical Water

Nore Stolte
Hong Kong University of Science and Technology https://orcid.org/0000-0002-2892-2133
Ding Pan (dingpan@ust.hk)
Hong Kong University of Science and Technology https://orcid.org/0000-0002-2353-0130

Article

Keywords:

Posted Date: April 5th, 2022

DOI: https://doi.org/10.21203/rs.3.rs-1478819/v1

Version of Record: A version of this preprint was published at Nature Communications on October 8th, 2022. See the published version at https://doi.org/10.1038/s41467-022-33696-w.

Nanoconfinement Facilitates Reactions of Carbon Dioxide in Supercritical Water

Nore Stolte[1] and Ding Pan[1,2,3,*]

[1]*Department of Physics, Hong Kong University of Science and Technology, Hong Kong, China*[†]

[2]*Department of Chemistry, Hong Kong University of Science and Technology, Hong Kong, China*

[3]*HKUST Fok Ying Tung Research Institute, Guangzhou, China*

(Dated: March 31, 2022)

Abstract

The reactions of CO_2 in water under extreme pressure-temperature conditions are of great importance to the carbon storage and transport below Earth's surface, which substantially affect the carbon budget in the atmosphere. Previous studies focus on the CO_2(aq) solutions in the bulk phase, but underground aqueous solutions are often confined to the nanoscale, and nanoconfinement and solid-liquid interfaces may substantially affect chemical speciation and reaction mechanisms, which are poorly known on the molecular scale. Here, we applied extensive ab initio molecular dynamics simulations to study aqueous carbon solutions nanoconfined by graphene and stishovite (SiO_2) at 10 GPa and 1000∼1400 K. We found that CO_2(aq) reacts more in nanoconfinement than in bulk. The stishovite-water interface makes the solutions more acidic, which shifts the chemical equilibria, and the interface chemistry also significantly affects the reaction mechanisms. Our findings suggest that CO_2(aq) in deep Earth may be more active than previously thought, and confining CO_2 and water in nanopores may enhance the efficiency of mineral carbonation.

INTRODUCTION

Aqueous fluids play a critical role in transporting carbon between Earth's surface and interior [1–3], which is a substantial part of Earth's carbon cycle, with great implications for global climate and human's energy consumption. It has long been assumed that aqueous carbon solutions under extreme pressure (P) and temperature (T) conditions are made by mixtures of neutral gas molecules [4], e.g., H_2O, CO_2, CH_4; however, recent studies showed that important chemical reactions may occur between water and carbon species, resulting in significant amounts of ionic products, which may further participate in water-rock interactions and the formation of diamonds in Earth's interior [5–11]. Most of the previous studies focus on properties of aqueous carbon solutions in the bulk phase. In fact, aqueous solutions in deep Earth are often confined to the nanoscale in pores, grain boundaries, and fractures of Earth's materials [12–14], where the physical and chemical properties of solutions may be dramatically different from those of bulk solutions. Additionally, in carbon capture and sequestration efforts, CO_2 mineralization occurring in water trapped in porous rocks offers an efficient and secure method to permanently store carbon underground with low risk of return to the atmosphere [15]. The behavior of aqueous carbon solutions under nanoconfinement at extreme P-T conditions is of great importance to the deep carbon cycle and CO_2 storage, but is poorly understood on the molecular scale.

Previous studies reported that nanoconfinement substantially affects properties of water, e.g., equation of state [16–18], phase behavior [19–21], dielectric constant [22–26], and diffusion [27–29]; as a result the reactivity of solutes under confinement may be very different from that in bulk solutions [30]. The dimensional reduction and increased fluid density may enhance reactions between small solutes in nanoconfinement [31, 32], whereas reactions involving large reactants or intermediates may be sterically hindered [33]. Further, the increase of the dielectric constant of nanoconfined water parallel to the confining surface leads to stabilization of charged aqueous reaction products [33], causing the enhanced autodisso-

ciation of water [23]. The solid-liquid interface also greatly affects the properties of confined aqueous solutions [34]. Preferential adsorption of solutes at the confining interface may shift reaction equilibria. For example, in the production of methane from carbon dioxide at hydrothermal vent conditions (CO_2 + 4 H_2 $\rightleftharpoons$ CH_4 + 2 H_2O), hydrophilic pore surfaces adsorb water, favoring the production of methane [35].

Nanoconfinement and interface chemistry may both likely change the properties of aqueous carbon solutions, but a molecular understanding is lacking on how chemical speciation and reaction mechanisms are affected. It was experimentally found that magnesite precipitates much faster in nanoscale water films than in bulk water [36]. Because it is very challenging to study aqueous solutions under nanoconfinement in experiment, atomistic simulations are widely used. Many studies applied classical force fields [27, 29, 34, 37], which were usually designed for bulk solutions at ambient conditions; their accuracy at extreme conditions is not well tested. As a comparison, ab initio molecular dynamics (AIMD) simulations do not rely on experimental input or empirical parameters [38–40]. We solve the many-body electronic structure numerically, so the breaking and forming of chemical bonds, electronic polarizability, and charge transfer are all treated at the quantum mechanical level [40, 41]. The AIMD method is widely considered as one of the most reliable methods to make predictions, and many simulations results were later confirmed by experiments [40, 41].

Here, we performed extensively long AIMD simulations to study CO_2(aq) solutions nanoconfined by graphene and stishovite (SiO_2) at 10 GPa and 1000$\sim$1400 K. These P-T conditions are typically found in Earth's upper mantle. We compared the CO_2(aq) reactions in nanoconfinement with those in the bulk solutions, and examined how weak and strong interactions between confining walls and confined solutions may affect chemical speciation and reaction mechanisms. Our work is of great importance to the carbon transformation in deep Earth, and also helps us to understand atomistic mechanisms of CO_2 mineralization in the carbon capture and storage.

RESULTS AND DISCUSSION

We first studied CO_2(aq) solutions confined by two graphene sheets at ∼10 GPa, and 1000∼1400 K (see Fig. 1(a)). The graphene sheet separation was 9.0 and 9.2 Å at 1000 K and 1400 K, respectively. The graphene sheets were modeled using a distance-dependent potential acting on the carbon and oxygen atoms, which was fitted to the interaction energies calculated using diffusion quantum Monte Carlo [42] and van der Waals density functional theory [43] (see Fig. S1 in the supporting information). We calculated the pressure of the confined solutions parallel to the graphene sheets, which are ∼10 GPa, consistent with the equation of state (see Table SI in the supporting information). In addition, We also used the atom number density profiles to calculate the actual volumes that aqueous carbon solutions occupy, and then applied the equation of state of CO_2 and water mixtures to obtain the pressures [44].

We directly dissolved the CO_2 molecules in the supercritical water, and the initial mole fraction of CO_2(aq) is 0.185. The CO_2 molecules reacted frequently with water, and we performed long AIMD simulations until the concentrations of carbon species reached equilibrium, which took 180∼480 ps (see Fig. S2 in the supporting information). Initially, the reaction between CO_2(aq) and H_2O produces bicarbonate ions (HCO_3^-):

$$CO_2(aq) + 2H_2O \rightleftharpoons HCO_3^- + H_3O^+. \quad (1)$$

This reaction may occur in one step, or involves dissociation of water so that OH^- can react with CO_2(aq) to form HCO_3^-(aq). The generated bicarbonate ion may further accept a proton to become a carbonic acid molecule (H_2CO_3(aq)), or may lose a proton to become a carbonate ion (CO_3^{2-}(aq)). The major carbon species in the solutions are CO_2, CO_3^{2-}, HCO_3^-, and H_2CO_3.

We compared the chemical speciation of the solutions under nanoconfinement and in the bulk phase at the same P-T conditions [10]. Fig. 2 shows that at 1000 K, the mole percent of CO_2(aq) in total dissolved carbon under nanoconfinement is 1.3±0.9%, whereas

it is 15.2±2.0% in the bulk solution. The mole percent of HCO_3^- under the nanoconfinement (50.0±1.0%) is higher than that in the bulk solution (35.9±0.7%), and the concentrations of H_2CO_3(aq) are similar (42.7±1.7% vs. 46.8±1.5%). With increasing temperature from 1000 K to 1400 K, the mole percents of CO_2(aq) under nanoconfinement and in the bulk solution increase to 14.5±3.2% and 58.8±2.0%, respectively. The equilibrium concentrations of CO_2(aq) in the nanoconfined solutions are lower than those in the bulk solutions at the two temperature conditions studied here, suggesting that nanoconfinement promotes the CO_2(aq) reactions. When increasing temperature along the isobar, due to thermal entropy effects, small molecules like CO_2(aq) are more favored. We did not see obvious difference in reaction rates between the nanoconfined and bulk solutions.

To understand why the nanoconfinement promotes the CO_2(aq) reactions, we analyzed the water structure in Fig. 3. In the graphene-confined solutions, there are two sharp density peaks for oxygen atoms, corresponding to two water layers (Fig. 3(a) and (b)). We found that the carbon-containing ions and molecules in these two layers tend to align parallel to the graphene sheets (see Fig. 4), and CO_2(aq) mostly reacts with water molecules in the same layer (Fig. S4 in the supporting information). Nanoconfinement increases the probability of reactive encounters between CO_2(aq) and solvent molecules, as diffusion is restricted to two dimensions [33]. It has been reported that the dielectric constant of nanoconfined water in the direction parallel to the confining surfaces, $\epsilon_{\parallel}$, increases significantly compared to the bulk value, and consistently water molecules dissociate more easily under nanoconfinement [23, 25]. Here, the produced OH^- ions from the water self-ionization may readily react with CO_2(aq) (reaction (1)), and the enhancement of $\epsilon_{\parallel}$ also further stabilizes the generated HCO_3^- and CO_3^{2-} ions. As a result, more CO_2(aq) molecules react under nanoconfinement than in the bulk.

After studying the effects of graphene nanoconfinement, we turned to the confinement by a realistic mineral in deep Earth, stishovite, which is a stable phase of SiO_2 (space group: $P4_2/mnm$) at the P-T conditions studied here [45, 46] and a major component of

subducted oceanic crust [47], playing a substantial role in transporting water into Earth's mantle [48]. We exposed the cleaved stishovite (100) face, one of the low-energy surfaces [49], to the carbon solutions as shown in Fig. 1(b). We carried out constant-pressure (NPT) simulations to keep the pressure perpendicular to the solid-liquid interface at ∼10 GPa, and then we found that the distance between the outermost oxygen atoms in two stishovite (100) surfaces is ∼7 Å (see Table S1 in the supporting information).

Fig. 2 shows the chemical speciation of aqueous carbon solutions under the stishovite confinement at ∼10 GPa and 1000∼1400 K. We found that at chemical equilibrium, 48.5±2.1% (1000 K) and 19.1±3.1% (1400 K) of carbon species, mostly HCO_3^- and CO_3^{-2}, are bonded to the stishovite surfaces, unlike in the graphene-confined solutions. In the atomic density profiles shown in Fig. 3(c) and (d), there are oxygen and carbon density peaks near the SiO_2 surfaces, where the oxygen and carbon atoms come from the solutions, indicating that the solid-liquid interface plays an important role.

In bulk stishovite crystals, silicon atoms are octahedrally coordinated, and oxygen atoms are trigonally coordinated, whereas at the cleaved stishovite (100) surface, silicon atoms form bonds with five oxygen atoms, and each oxygen atom bridges two undercoordinated silicon atoms. Water molecules may dissociate or bond at the stishovite surface. The hydroxide ion (OH^-) from water dissociation can bond to an undercoordinated silicon atom to form a silanol (Si-OH) group, and the extra proton can bond with the surface oxygen atom to become a Si-(OH^+)-Si bridge (see Fig. 3(e–g)). Similar hydroxylation occurs at the quartz (1000) surface [50, 51]. The hydroxyl groups at the stishovite surface may react with CO_2(aq) to form HCO_3^- (Fig. 5(a)). The surface hydroxyl groups or the undercoordinated oxygen atoms may also accept protons released in reaction (1), driving the reaction forward (Fig. 5(b)).

We analyzed the spatial orientation of the sp^2 carbon species such as CO_3^{2-}(aq), HCO_3^-(aq), and H_2CO_3(aq) in the stishovite-confined solutions in Fig. 4(c) and (d). We found that the molecular plane of the sp^2 carbon species bonded to the stishovite surface tends to form an

angle of ∼60° or ∼90° with the solid-liquid interface plane, dramatically different from the orientation of carbon species in the graphene-confined solutions. When the angle is ∼60°, the carbon species has two Si-O bonds by straddling two silicone atoms (Fig. 4(e)), while with the angle of ∼90° the carbon species forms only one Si-O bond (Fig. 4(f)). The strong solid-liquid interaction substantially affects the molecular structure of the confined carbon solutions.

After analyzing the carbon species at the solid-liquid interface, we investigated the carbon species not bonded to the stishovite surface, i.e., fully dissolved in the stishovite-confined solutions. Fig. 2 show that at 1000 K, the mole percent of dissolved CO_2(aq) is 10.5±2.3%, which is larger than 1.3±0.9% in the graphene-confined solution, and slightly smaller than 15.1±2.0% in the bulk solution. At 1400 K, the mole percent of dissolved CO_2(aq) in the stishovite-confined solution (39.8±3.6%) is also between those in the graphene-confined (14.5±3.2%) and bulk (58.8±2.0%) solutions.

Both hydroxide ions and protons may be chemically adsorbed on the SiO_2 surface, which affects the acidity of carbon solutions. Considering that the pH value of neutral water is no longer 7 under extreme P-T conditions, we calculated the difference between pH and pOH to quantify the acidity of solutions [52]:

$$f = \mathrm{pH} - \mathrm{pOH} = -\log_{10}\left(\frac{[\mathrm{H_3O^+}]}{[\mathrm{OH^-}]}\right), \tag{2}$$

where $[H_3O^+]$ and $[OH^-]$ are the concentrations of hydronium and hydroxide ions, respectively. Because CO_2(aq) reacts with water to generate H_3O^+, the solutions studied here are all acidic, i.e., $f < 0$, as shown in Table I. The interesting finding is that the f value of stishovite-confined solutions is more negative than that of graphene-confined solutions at the same P-T conditions, which means that the former is more acidic than the latter, even though less CO_2(aq) reacts in the stishovite-confined solutions. We have discussed that the stishovite surface adsorbs the hydroxide ions and protons from solutions. Additionally, our AIMD trajectories show that the SiO_2 surface favors the adsorption of OH^- over that of

H^+ (Fig. S5 in the supporting information); as a result, the stishovite-confined solutions are more acidic than the graphene-confined ones at the same P-T conditions. Increasing the concentration of H_3O^+ shifts the equilibrium of reaction (1) towards the left, so there is more CO_2(aq) in the solutions.

The nanoconfinement enhances $\epsilon_{\|}$, which stabilized charged ions, so in both graphene- and stishovite-confined solutions, more CO_2(aq) reacts. However, it has been reported that $\epsilon_{\|}$ near the hydrophobic surface increases more than near the hydrophilic surface, because the motion of water molecules are more hindered at the the hydrophilic surface [22]. Considering that the stishovite surface is more hydrophilic than graphene, charged ions are less stabilized, so we found more CO_2(aq) in the stishovite-confined solutions than in the graphene-confined solutions. Therefore, the CO_2 concentration increase in the stishovite-confined solutions is a combined result of the hydrophilic confinement and the adsorption preference of OH^- on the stishovite (100) surface.

In our simulations, we used the semilocal Perdew-Burke-Ernzerhof (PBE) exchange-correlation (xc) functional [53], which was reported insufficient to describe aqueous systems at ambient conditions [54]; however, our previous studies showed that PBE performed better for the equation of state and dielectric properties of water [55, 56] and the carbon speciation in water [7] at extreme P-T conditions than at ambient conditions. Particularly, we compared the simulations using PBE and a hybrid xc functional, PBE0 [57]. For an aqueous carbon solution at $\sim$11 GPa and 1000 K, whose initial mole fraction of CO_2(aq) is 0.016, both PBE and PBE0 suggest that HCO_3^- is the dominant carbon species, and its mole percents are 79.8% and 75.0%, respectively [7].

CONCLUSION

We performed extensively long AIMD simulations to study the chemical reactions and speciation of aqueous carbon solutions nanoconfined by graphene and stishovite at 10 GPa

and 1000∼1400 K. We found that the graphene nanoconfinement promotes the CO_2(aq) reactions. When graphene is replaced by stishovite, less CO_2(aq) reacts, but still more than in the bulk solutions. We found that contacting the stishovite (100) surface makes the solutions more acidic, which shifts the chemical equilibria, though the stishovite surface also catalyzes the CO_2(aq) reactions by adsorbing HCO_3^- and H^+.

The enhanced reactivity of CO_2(aq) in nanoconfinement has important implications for carbon transport and fluid-rock interactions in deep Earth. Aqueous fluids located at grain boundaries in minerals can either exist in isolated fluid-filled pores, or form a connected network of channels along grains facilitating fluid transport [13]. It is known that adding molecular CO_2(aq) to water may increase the rock-fluid-rock dihedral angle θ, which inhibits fluid flow [58, 59]. However, our study shows that CO_2(aq) reacts with water under nanoconfinement and could react with the solid interface, which may decrease θ and promote interconnectivity of fluids [14]. Our study also sheds light on atomistic mechanisms of CO_2 storage through mineral carbonation. CO_2 reacts more in nanoconfined water, which benefits the CO_2 mineralization. If we choose minerals with larger points of zero charge than that of SiO_2, such as forsterite [60] and magnesium oxide [61], the CO_2 reactivity may be further enhanced.

METHODS

We carried out Born-Oppenheimer ab initio molecular dynamics using the Qbox package [62]. We used periodic boundary conditions and employed plane-wave basis sets and norm-conserving pseudopotentials [63, 64], with a plane-wave cutoff of 85 Ry. The cutoff was increased to 145 Ry for pressure calculations. We applied density functional theory and the PBE exchange-correlation functional [53]. We sampled the Brillouin zone at the Γ point. We performed AIMD simulations in the canonical, i.e., NVT, ensemble. Stochastic velocity rescaling was used to control the temperature [65], with a damping factor of 24.2 fs. We

replaced hydrogen by deuterium to use a large time step of 0.24 fs in the simulations, but still referred to these atoms as H atoms.

We ran simulations for 180–480 ps after 20 ps equilibration to reach chemical equilibrium. We analyzed the AIMD trajectories to determine the nature of carbon-containing molecules. For each carbon atom, we searched for the three nearest oxygen atoms, and sorted the C-O distances in increasing order. If the difference between the second and third C-O distance is less than 0.4 Å, the carbon species is a CO_3^{2-} ion; otherwise, it is CO_2. Hydrogen atoms were considered being bonded to their nearest-neighbor oxygen atoms. For the solutions confined by stishovite, the oxygen atoms were considered bonded to silicon atoms when the interatomic distance fell within the first peak of the Si-O_{aq} radial distribution function (RDF), i.e., 2.6 Å (Fig. S3 in the supporting information).

ACKNOWLEDGEMENTS

N.S. acknowledges the Hong Kong Ph.D. Fellowship Scheme. D.P. acknowledges support from the Croucher Foundation through the Croucher Innovation Award, Hong Kong Research Grants Council (Projects ECS-26305017, GRF-16307618, and GRF-16306621), National Natural Science Foundation of China (Project 11774072 and Excellent Young Scientists Fund), and the Alfred P. Sloan Foundation through the Deep Carbon Observatory. Part of this work was carried out using computational resources from the National Supercomputer Center in Guangzhou, China.

CONTRIBUTIONS

D.P. designed the research. Calculations were performed by N.S. All authors contributed to the analysis and discussion of the data and the writing of the manuscript.

* dingpan@ust.hk

† Present address: Lehrstuhl für Theoretische Chemie, Ruhr-Universität Bochum, 44780 Bochum, Germany

[1] Peacock, S. M. Fluid processes in subduction zones. *Science* **248**, 329–337 (1990).

[2] Kelemen, P. B. & Manning, C. E. Reevaluating carbon fluxes in subduction zones, what goes down, mostly comes up. *Proc. Natl. Acad. Sci. U. S. A.* **112**, E3997–E4006 (2015).

[3] Manning, C. E. & Frezzotti, M. L. Subduction-zone fluids. *Elements* **16**, 395–400 (2020).

[4] Zhang, C. & Duan, Z. A model for C-O-H fluid in the Earth's mantle. *Geochim. Cosmochim. Acta* **73**, 2089–2102 (2009).

[5] Facq, S., Daniel, I., Montagnac, G., Cardon, H. & Sverjensky, D. A. In situ Raman study and thermodynamic model of aqueous carbonate speciation in equilibrium with aragonite under subduction zone conditions. *Geochim. Cosmochim. Acta* **132**, 375–390 (2014).

[6] Sverjensky, D. A., Stagno, V. & Huang, F. Important role for organic carbon in subduction-zone fluids in the deep carbon cycle. *Nat. Geosci.* **7**, 909–913 (2014).

[7] Pan, D. & Galli, G. The fate of carbon dioxide in water-rich fluids under extreme conditions. *Sci. Adv.* **2**, e1601278 (2016).

[8] Abramson, E. H., Bollengier, O. & Brown, J. M. The water-carbon dioxide miscibility surface to 450 °C and 7 GPa. *Am. J. Sci.* **317**, 967–989 (2017).

[9] Manning, C. E. Fluids of the lower crust: Deep is different. *Annu. Rev. Earth Planet. Sci.* **46**, 67–97 (2018).

[10] Stolte, N. & Pan, D. Large presence of carbonic acid in CO_2-rich aqueous fluids under Earth's mantle conditions. *J. Phys. Chem. Lett.* **10**, 5135–5141 (2019).

[11] Stolte, N., Yu, J., Chen, Z., Sverjensky, D. A. & Pan, D. Water–gas shift reaction produces formate at extreme pressures and temperatures in deep earth fluids. *J. Phys. Chem. Lett.* **12**,

4292–4298 (2021).

[12] Gautam, S. S., Ok, S. & Cole, D. R. Structure and dynamics of confined C-O-H fluids relevant to the subsurface: Application of magnetic resonance, neutron scattering, and molecular dynamics simulations. *Front. Earth Sci.* **5**, 43 (2017).

[13] Marquardt, K. & Faul, U. H. The structure and composition of olivine grain boundaries: 40 years of studies, status and current developments. *Phys. Chem. Miner.* **45**, 139–172 (2018).

[14] Huang, Y., Nakatani, T., Nakamura, M. & McCammon, C. Experimental constraint on grain-scale fluid connectivity in subduction zones. *Earth Planet. Sci. Lett.* **552**, 116610 (2020).

[15] Snæbjörnsdóttir, S. Ó. *et al.* Carbon dioxide storage through mineral carbonation. *Nat. Rev. Earth Environ.* **1**, 90–102 (2020).

[16] Günther, G., Prass, J., Paris, O. & Schoen, M. Novel insights into nanopore deformation caused by capillary condensation. *Phys. Rev. Lett.* **101**, 086104 (2008).

[17] Long, Y., Palmer, J. C., Coasne, B., Śliwinska-Bartkowiak, M. & Gubbins, K. E. Pressure enhancement in carbon nanopores: A major confinement effect. *Phys. Chem. Chem. Phys.* **13**, 17163–17170 (2011).

[18] Hartkamp, R., Ghosh, A., Weinhart, T. & Luding, S. A study of the anisotropy of stress in a fluid confined in a nanochannel. *J. Chem. Phys.* **137**, 044711 (2012).

[19] Algara-Siller, G. *et al.* Square ice in graphene nanocapillaries. *Nature* **519**, 443–445 (2015).

[20] Chen, J., Schusteritsch, G., Pickard, C. J., Salzmann, C. G. & Michaelides, A. Two dimensional ice from first principles: Structures and phase transitions. *Phys. Rev. Lett.* **116**, 025501 (2016).

[21] Gao, Z., Giovambattista, N. & Sahin, O. Phase diagram of water confined by graphene. *Sci. Rep.* **8**, 6228 (2018).

[22] Bonthuis, D. J., Gekle, S. & Netz, R. R. Dielectric profile of interfacial water and its effect on double-layer capacitance. *Phys. Rev. Lett.* **107**, 166102 (2011).

[23] Muñoz-Santiburcio, D. & Marx, D. Nanoconfinement in slit pores enhances water self-dissociation. *Phys. Rev. Lett.* **119**, 056002 (2017).

[24] Fumagalli, L. *et al.* Anomalously low dielectric constant of confined water. *Science* **360**, 1339–1342 (2018).

[25] Ruiz-Barragan, S., Muñoz-Santiburcio, D., Körning, S. & Marx, D. Quantifying anisotropic dielectric response properties of nanoconfined water within graphene slit pores. *Phys. Chem. Chem. Phys.* **22**, 10833–10837 (2020).

[26] Deißenbeck, F., Freysoldt, C., Todorova, M., Neugebauer, J. & Wippermann, S. Dielectric properties of nanoconfined water: A canonical thermopotentiostat approach. *Phys. Rev. Lett.* **126**, 136803 (2021).

[27] Chiavazzo, E., Fasano, M., Asinari, P. & Decuzzi, P. Scaling behaviour for the water transport in nanoconfined geometries. *Nat. Commun.* **5**, 3565 (2014).

[28] Thompson, W. H. Perspective: Dynamics of confined liquids. *J. Chem. Phys.* **149**, 170901 (2018).

[29] Phan, A. & Striolo, A. Evidence of facilitated transport in crowded nanopores. *J. Phys. Chem. Lett.* **11**, 1814–1821 (2020).

[30] Muñoz-Santiburcio, D. & Marx, D. Confinement-controlled aqueous chemistry within nanometric slit pores. *Chem. Rev.* **121**, 6293–6320 (2021).

[31] Turner, C. H., Johnson, J. K. & Gubbins, K. E. Effect of confinement on chemical reaction equilibria: The reactions $2NO \Leftrightarrow (NO)_2$ and $N_2 + 3H_2 \Leftrightarrow 2NH_3$ in carbon micropores. *J. Chem. Phys.* **114**, 1851–1859 (2001).

[32] Santiso, E. E. *et al.* Adsorption and catalysis: The effect of confinement on chemical reactions. *Appl. Surf. Sci.* **252**, 766–777 (2005).

[33] Muñoz-Santiburcio, D. & Marx, D. Chemistry in nanoconfined water. *Chem. Sci.* **8**, 3444–3452 (2017).

[34] Phan, A., Cole, D. R. & Striolo, A. Preferential adsorption from liquid water-ethanol mixtures in alumina pores. *Langmuir* **30**, 8066–8077 (2014).

[35] Le, T., Striolo, A., Turner, C. H. & Cole, D. R. Confinement effects on carbon dioxide methanation: A novel mechanism for abiotic methane formation. *Sci. Rep.* **7**, 9021 (2017).

[36] Miller, Q. R. S. *et al.* Anomalously low activation energy of nanoconfined $MgCO_3$ precipitation. *Chem. Commun.* **55**, 6835–6837 (2019).

[37] Cole, D. R., Chialvo, A. A., Rother, G., Vlcek, L. & Cummings, P. T. Supercritical fluid behavior at nanoscale interfaces: Implications for CO_2 sequestration in geologic formations. *Philos. Mag.* **90**, 2339–2363 (2010).

[38] Car, R. & Parrinello, M. Unified approach for molecular dynamics and density-functional theory. *Phys. Rev. Lett.* **55**, 2471–2474 (1985).

[39] Galli, G. & Parrinello, M. Ab-initio molecular dynamics: Principles and practical implementation. In Meyer, M. & Pontikis, V. (eds.) *Computer Simulation in Materials Science*, 283–304 (Springer, 1991).

[40] Marx, D. & Hutter, J. *Ab Initio Molecular Dynamics: Basic Theory and Advanced Methods* (Cambridge University Press, 2009).

[41] Gygi, F. & Galli, G. Ab initio simulation in extreme conditions. *Mater. Today* **8**, 26–32 (2005).

[42] Brandenburg, J. G. *et al.* Physisorption of water on graphene: Subchemical accuracy from many-body electronic structure methods. *J. Phys. Chem. Lett.* **10**, 358–368 (2019).

[43] Takeuchi, K. *et al.* Adsorption of CO_2 on graphene: A combined TPD, XPS, and vdW-DF study. *J. Phys. Chem. C* **121**, 2807–2814 (2017).

[44] Duan, Z. & Zhang, Z. Equation of state of the H_2O, CO_2, and H_2O-CO_2 systems up to 10 GPa and 2573.15 K: Molecular dynamics simulations with ab initio potential surface. *Geochim. Cosmochim. Acta* **70**, 2311–2324 (2006).

[45] Akaogi, M., Yusa, H., Shiraishi, K. & Suzuki, T. Thermodynamic properties of α-quartz, coesite, and stishovite and equilibrium phase relations at high pressures and high temperatures. *J. Geophys. Res. Solid Earth* **100**, 22337–22347 (1995).

[46] Zhang, J., Li, B., Utsumi, W. & Liebermann, R. C. In situ X-ray observations of the coesite-stishovite transition: Reversed phase boundary and kinetics. *Phys. Chem. Miner.* **23**, 1–10 (1996).

[47] Aoki, I. & Takahashi, E. Density of MORB eclogite in the upper mantle. *Phys. Earth Planet. Inter.* **143–144**, 129–143 (2004).

[48] Lin, Y., Hu, Q., Meng, Y., Walter, M. & Mao, H.-K. Evidence for the stability of ultrahydrous stishovite in Earth's lower mantle. *Proc. Natl. Acad. Sci. U. S. A.* **117**, 184–189 (2020).

[49] Feya, O. D. *et al.* Tetrahedral honeycomb surface reconstructions of quartz, cristobalite and stishovite. *Sci. Rep.* **8**, 11947 (2018).

[50] Adeagbo, W. A., Doltsinis, N. L., Klevakina, K. & Renner, J. Transport processes at α-quartz-water interfaces: Insights from first-principles molecular dynamics simulations. *ChemPhysChem* **9**, 994–1002 (2008).

[51] Ledyastuti, M., Liang, Y. & Matsuoka, T. The first-principles molecular dynamics study of quartz-water interface. *Int. J. Quantum Chem.* **113**, 401–412 (2013).

[52] Dettori, R. & Donadio, D. Carbon dioxide, bicarbonate and carbonate ions in aqueous solutions under deep Earth conditions. *Phys. Chem. Chem. Phys.* **22**, 10717–10725 (2020).

[53] Perdew, J. P., Burke, K. & Ernzerhof, M. Generalized gradient approximation made simple. *Phys. Rev. Lett.* **77**, 3865–3868 (1996).

[54] Gillan, M. J., Alfè, D. & Michaelides, A. Perspective: How good is DFT for water? *J. Chem. Phys.* **144**, 130901 (2016).

[55] Pan, D., Spanu, L., Harrison, B., Sverjensky, D. A. & Galli, G. Dielectric properties of water under extreme conditions and transport of carbonates in the deep Earth. *Proc. Natl. Acad. Sci. U. S. A.* **110**, 6646–6650 (2013).

[56] Pan, D., Wan, Q. & Galli, G. The refractive index and electronic gap of water and ice increase with increasing pressure. *Nat. Commun.* **5**, 3919 (2014).

[57] Adamo, C. & Barone, V. Toward reliable density functional methods without adjustable parameters: The PBE0 model. *J. Chem. Phys.* **110**, 6158–6170 (1999).

[58] Watson, E. B. & Brenan, J. M. Fluids in the lithosphere, 1. Experimentally-determined wetting characteristics of CO_2-H_2O fluids and their implications for fluid transport, host-rock physical properties, and fluid inclusion formation. *Earth Planet. Sci. Lett.* **85**, 497–515 (1987).

[59] Holness, M. B. Equilibrium dihedral angles in the system quartz-CO_2-H_2O-NaCl at 800 °C and 1–15 kbar: The effects of pressure and fluid composition on the permeability of quartzites. *Earth Planet. Sci. Lett.* **114**, 171–184 (1992).

[60] Wogelius, R. A. & Walther, J. V. Olivine dissolution at 25 °C: Effects of pH, CO_2, and organic acids. *Geochim. Cosmochim. Acta* **55**, 943–954 (1991).

[61] Kosmulski, M. Isoelectric points and points of zero charge of metal (hydr)oxides: 50 years after Parks' review. *Adv. Colloid Interface Sci.* **238**, 1–61 (2016).

[62] Gygi, F. Architecture of Qbox: A scalable first-principles molecular dynamics code. *IBM J. Res. Dev.* **52**, 137–144 (2008).

[63] Hamann, D. R., Schlüter, M. & Chiang, C. Norm-conserving pseudopotentials. *Phys. Rev. Lett.* **43**, 1494–1497 (1979).

[64] Vanderbilt, D. Optimally smooth norm-conserving pseudopotentials. *Phys. Rev. B* **32**, 8412–8415 (1985).

[65] Bussi, G., Donadio, D. & Parrinello, M. Canonical sampling through velocity rescaling. *J. Chem. Phys.* **126**, 014101 (2007).

[66] Flyvbjerg, H. & Petersen, H. G. Error estimates on averages of correlated data. *J. Chem. Phys.* **91**, 461–466 (1989).

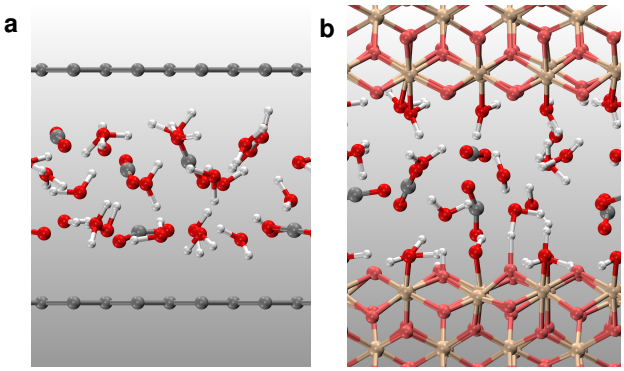

FIG. 1. Snapshots of ab initio molecular dynamics simulations under confinement. (**a**) CO_2(aq) confined by graphene sheets. (**b**) CO_2 confined by cleaved stishovite (SiO_2) (100) slabs. Red balls represent oxygen atoms in solutions, and pink balls are oxygen atoms in SiO_2. Gray, white, and yellow balls are carbon, hydrogen, and silicon atoms, respectively.

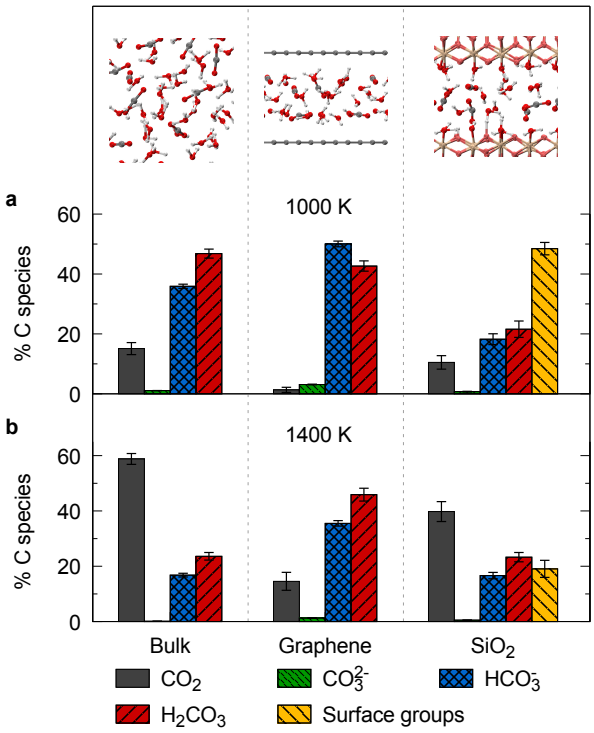

FIG. 2. Mole percents of carbon species in the CO_2(aq) solutions in the bulk and nanoconfined by graphene and stishovite (SiO_2) at chemical equilibrium. The initial mole fraction of CO_2(aq) is 0.185. The pressures in all solutions are ∼10 GPa. The temperatures are (**a**) 1000 K and (**b**) 1400 K. The data of bulk solutions in (**a**) are from Ref. [10], and the bulk data in (**b**) were interpolated using the simulation results in Ref. [10]. Uncertainties were obtained using the blocking method [66].

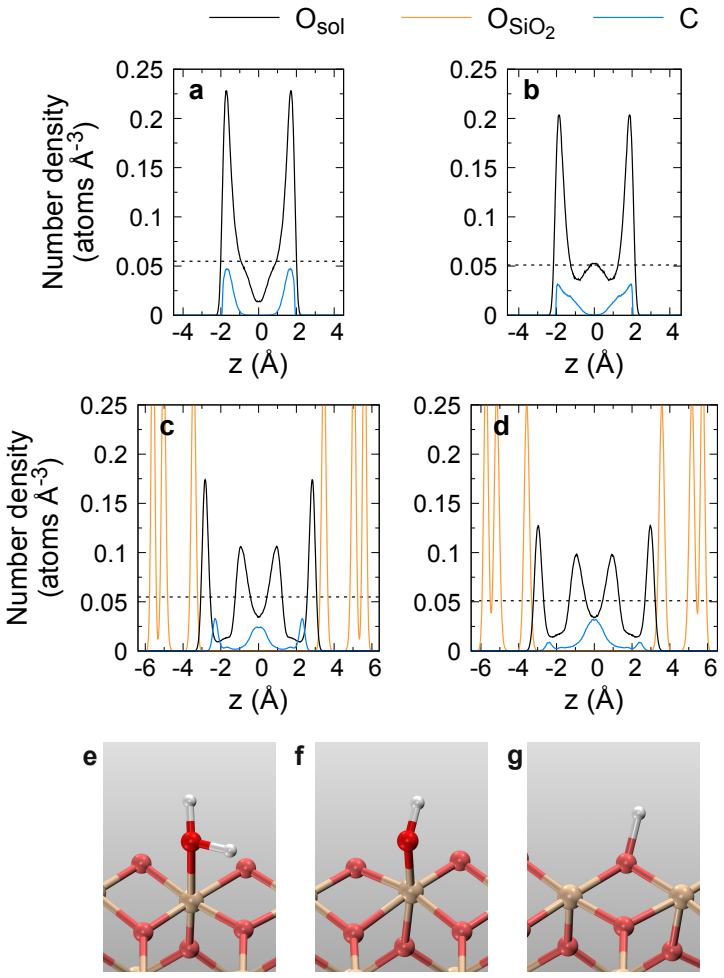

FIG. 3. Number density profiles of oxygen atoms (O_{sol}) and carbon atoms along the z axis, normal to the confining surfaces. (**a**) and (**b**) show the solutions under graphene confinement at 1000 and 1400 K, respectively. (**c**) and (**d**) show the solutions under stishovite confinement at 1000 and 1400 K, respectively. O_{SiO_2} refers to the oxygen atoms in stishovite. The pressures in all solutions are ∼10 GPa. The initial mole fraction of CO_2(aq) is 0.185. The center of confined fluids is set at $z = 0$, and the density distributions have been symmetrized. The horizontal black dashed lines represent the oxygen density in bulk solutions at the corresponding P-T conditions [44]. (**e**), (**f**), and (**g**) show the H_2O molecule, the OH^- and H^+ ions bonded to the stishovite (100) surface, respectively.

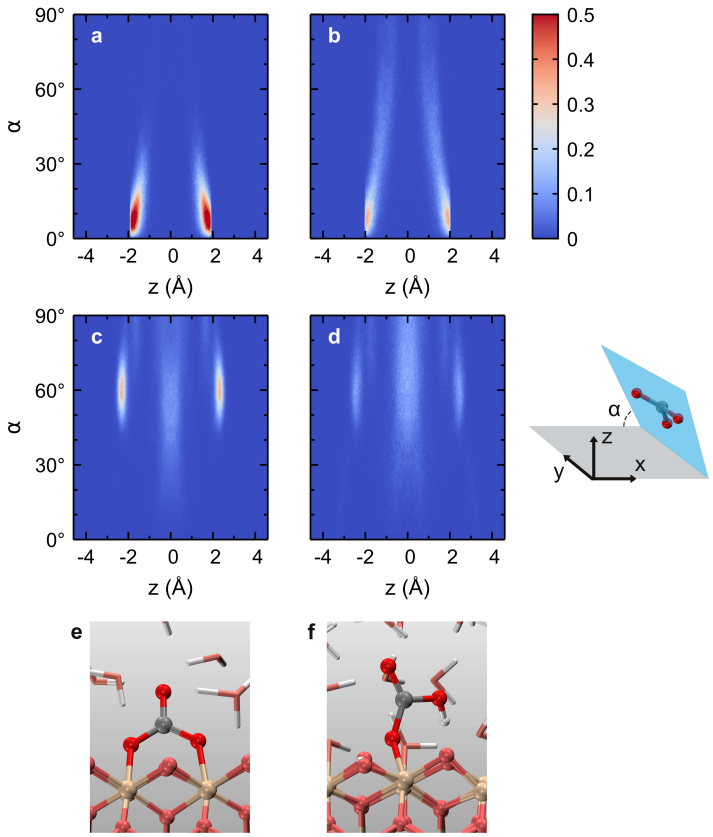

FIG. 4. Orientation distribution of sp^2 carbon species in CO_2(aq) solutions. The dihedral angle α is between the confinement interface and the plane defined by the three oxygen atoms in sp^2 carbon species. (**a**) and (**b**) show the solutions under graphene confinement at 1000 and 1400 K, respectively. (**c**) and (**d**) show the solutions under stishovite confinement at 1000 and 1400 K, respectively. The pressure in all solutions are ∼10 GPa. The initial mole fraction of CO_2(aq) is 0.185. The center of confined fluids is set at $z = 0$, and the angle distributions have been symmetrized. (**e**) and (**f**) show the CO_3^{2-} and HCO_3^- ions adsorbed on the stishovite (100) surface, respectively.

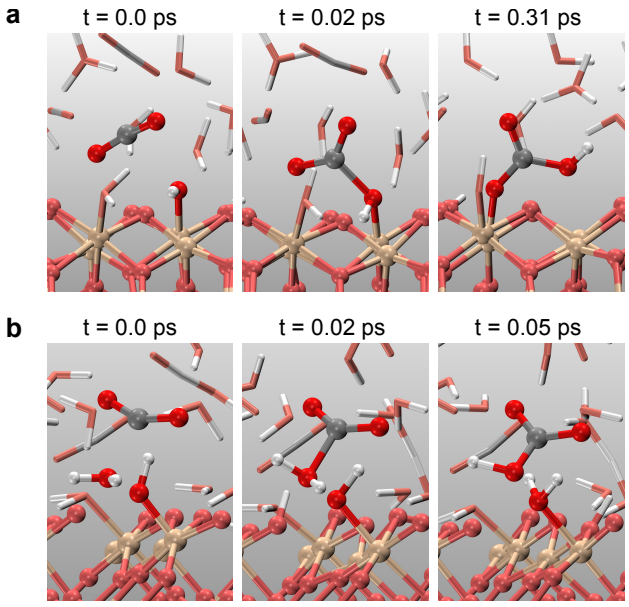

FIG. 5. Reaction of CO_2(aq) catalyzed by the stishovite (100) surface. (**a**) shows the formation of HCO_3^- at the interface. (**b**) shows the proton released from the reaction between CO_2(aq) and water is accepted by the silanol (Si-OH) surface group.

TABLE I. The acidity f of carbon aqueous solutions: $f = \mathrm{pH} - \mathrm{pOH}$. The initial mole fraction of CO_2(aq) is 0.185, and the pressures in the solutions are about 10 GPa. Uncertainties are obtained using the blocking method [66].

T	Confinement	f
1000 K	Graphene	-1.24 ± 0.02
	Stishovite	-1.46 ± 0.02
1400 K	Graphene	-0.94 ± 0.05
	Stishovite	-1.13 ± 0.03

Supplementary Files

This is a list of supplementary files associated with this preprint. Click to download.

- ConfinedCO2aqv2SI.pdf